Absolute Calibration of ACIS X-ray CCDs Using Calculable, Undispersed Synchrotron Radiation

M. W. Bautz,[a] M. J. Pivovaroff,[a] S. E. Kissel,[a] G. Y. Prigozhin,[a] T. Isobe,[b] S. E. Jones,[a] G. R. Ricker,[a] R. Thornagel,[c] S. Kraft,[c] F. Scholze,[c] and G. Ulm[c]

[a]MIT Center for Space Research, 77 Massachusetts Ave, Cambridge, MA 02139, USA
[b]Harvard-Smithsonian CfA/CXO, 60 Garden St. MS-34, Cambridge, MA 02139
[c]Physikalisch-Technische Bundesanstalt, Abbestr. 2-12, D-10587 Berlin, GERMANY

ABSTRACT

We have performed a series of measurements with the Physikalisch-Technische Bundesanstalt beamline of the electron storage ring BESSY I which provide the basis for the absolute calibration of the Advanced CCD Imaging Spectrometer (ACIS). ACIS is a prime focal plane instrument aboard the recently-launched *Chandra X-ray Observatory*. We have achieved an absolute detection efficiency knowledge accurate to better than 5% over the $0.3 - 4$ keV band. We describe our measurement and analysis techniques, including our detector response modeling and pileup corrections. We summarize a variety of external and internal consistency checks which provide the basis for our error estimates. We discuss the factors limiting the accuracy of our measurements.

Keywords: CCDs, X-rays, ACIS, Chandra

1. INTRODUCTION

A long-awaited new era in X-ray astronomy began last year with the launches of both *Chandra*[1] and *XMM-Newton*.[2] In order to maximize the scientific returns from these expensive missions, extensive ground calibration efforts have been undertaken for each of them. We have reported periodically[3–5] on various aspects of the calibration of *Chandra's* Advanced CCD Imaging Spectrometer (ACIS).[6] In this contribution we focus on the absolute calibration of *Chandra's* CCD detectors.

The ACIS focal plane contains ten CCD detectors designed and fabricated at MIT Lincoln Laboratory.[7] These detectors (model CCID17) are frame-transfer devices with 1024 by 1026 pixels in the active region; each pixel is 24 μm square. As operated in ACIS, the front-illuminated devices have system noises of $2 - 3$ electrons, RMS and depletion depths of $\sim$70 μm.[4] Eight of the ten ACIS detectors are front-illuminated; the other two detectors are back-illuminated. In this contribution we focus exclusively on the calibration of the front-illuminated detectors.

We have used the calculable undispersed synchrotron radiation at the Physikalisch-Technische Bundesanstalt (PTB) beamline at BESSY I as our primary radiometric standard. For logistical reasons it proved impractical to calibrate the flight detectors directly at PTB, so we have instead calibrated flight-like ACIS CCDs there. These absolutely calibrated detectors were then used as transfer standards in our laboratory at MIT to determine the efficiency of the flight devices. Subsequent measurements with the integrated ACIS instrument have allowed us to check the accuracy of the fundamental calibration. The calibration concept is illustrated in Figure 1.

In this paper we describe the measurement method in greater detail and present the results of the absolute calibration of ACIS transfer standard detectors. We discuss the measurement and modeling errors which limit the accuracy of these calibrations, and estimate the final calibration accuracy of the flight detectors at the time *Chandra's* launch.

2. MEASUREMENTS

The laboratory of the Physikalisch-Technische Bundesanstalt (PTB) at the BESSY I electron storage ring provided a broad-band ($0.1 - 4$ keV) source radiation source of calculable intensity.[8] The spectral flux was calculable with relative uncertainty below 1% from knowledge of the geometry of the detector with respect to the orbital plane, the electron energy, ring current and magnetic field of the bending magnets.

Further author information: MWB: E-mail: mwb@drang.mit.edu; MJP: E-mail: mjp@space.mit.edu

In *X-Ray Optics, Instruments, and Missions III*, Joachim E. Trümper, Bernd Aschenbach, Editors,
Proceedings of SPIE Vol. 4012 (2000) • 0277-786X/00/$15.00

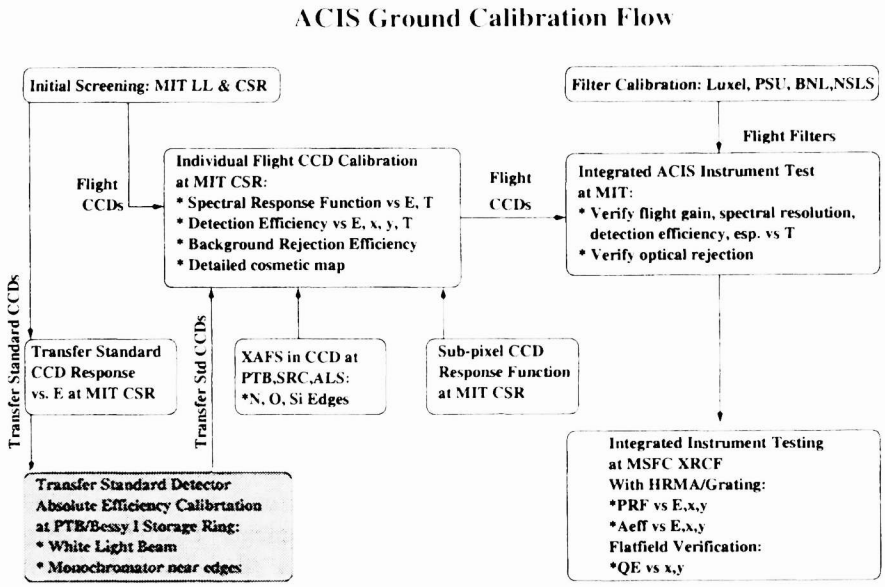

Figure 1. ACIS ground calibration flow. This paper focused on the measurements listed in the shaded box.

Figure 2 illustrates the experimental set-up at the PTB laboratory. A standard MIT vacuum chamber, modified to hold two CCDs simultaneously, was mounted to the PTB beamline via a ceramic electro-isolator to eliminate electrical interference between the CCD electronics and the BESSY facility. A gate valve and turbo pump located between the CCDs and the storage ring allowed the chamber to be connected and pumped down to the requisite vacuum without compromising the integrity of the storage ring. The CCDs were operated at the nominal flight temperature of -120 C°.

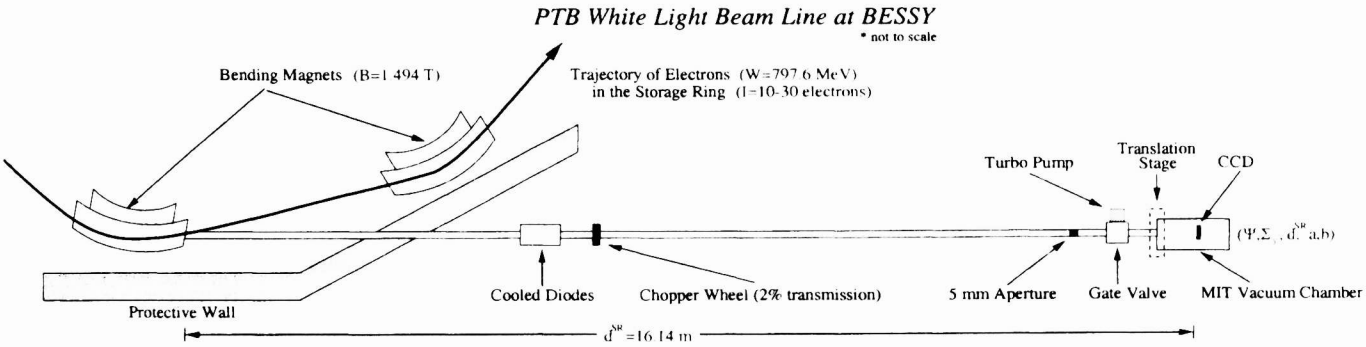

Figure 2. Sketch of the PTB laboratory, showing the basic geometry of the beamline and the interface between it and the CCDs.

Even a single electron in the storage ring would produce a flux high enough to cause significant pileup (that is, more than one photon would have interacted in a pixel during a single CCD exposure) that would have degraded the calibration accuracy. Two measures were taken to reduce the flux to an acceptable level. First, a chopper wheel with a 2.00% transmission was inserted into the beam line to limit the incident flux. Second, the CCD exposure time was decreased by reading out only 256 of the 1026 rows in the device. This readout mode reduced the exposure time by a factor of four. Even with these measures in place, it was necessary to operate the storage ring at very low current. Typical currents ranged from 10 to 30 electrons, although measurements with as few as 5 electrons and as many as 50 electrons were performed to calibrate pileup effects.

One consequence of using the chopper wheel is that synchrotron flux is no longer continuously incident upon the CCD. Instead, discrete flashes of light are seen during a single frametime. As the readout electronics were not synchronized with the chopper wheel frequency, the number of flashes varied between two integer values. The number

of frames is known, so to determine the total observation time (a step necessary to check the normalization), we must determine how frequently N or $N+1$ flashes were seen to calculate an effective exposure time. Two different types of electronics were used for data collection, one of which has a readout twice that of the other. This faster readout only allowed either five or six flashes per frametime, complicating the exposure time calculation and introducing a 0.1% uncertainty into its value. Refer to §3.4 for additional details.

The process of reading out 256 rows of the CCD limited the amount of the detector that could be calibrated during one measurement. To ensure that all the incident photons would fall on an active area of the detector (a necessary requirement for the determination of absolute quantum efficiency) a five mm high aperture was placed in the beam line and carefully centered on the electron orbital plane. The five mm slit produced an illumination pattern 216 pixels tall, and the CCD columns were nominally aligned perpendicular to the orbital plane. The detector chamber was mounted to a two dimensional translation stage fitted to the end of the PTB beamline. To calibrate an entire detector, the chamber was moved an appropriate distance in the y direction, a 256-row swath of the CCD was read out, and the image was visually inspected to check that all the photons hit the active area. This procedure was repeated four or five times to calibrate the entire chip. The chamber was then moved in the horizontal direction to illuminate a second CCD inside the chamber. By placing two chips inside the chamber, the overhead associated with thermally cycling the CCD, venting the chamber, switching CCDs, re-evacuating the chamber and finally cooling the CCDs was reduced. This configuration allowed calibration of as many as four chips in a single 48-hour period.

At least once in each measurement period accurate measurements of the bending magnetic field were made, using methods described by Arnold & Ulm[8] and references therein. To continuously monitor the electron beam current, four Si photodiodes were placed in the direct synchrotron radiation in the PTB beamline as near as possible to the storage ring. The photodiodes were cooled to liquid nitrogen temperature to reduce dark current noise. The photo-current decreased in obvious steps with the occasional loss of one of the stored electrons, thus allowing the number of the stored electrons to be determined without uncertainty.

Given these parameters, the synchrotron radiation from the storage ring can be derived by Schwinger's equation[9,10]:

$$I(\lambda)^{SR} = I^{SR,\parallel}(\lambda) + I^{SR,\perp}(\lambda) = \frac{2e\rho^2 I}{3\varepsilon_0\lambda^4\gamma^4\cos\psi}\left\{ [1+(\gamma\psi)^2]^2 K_{\frac{2}{3}}^2(\xi) + [1+(\gamma\psi)^2]^2(\gamma\psi)^2 K_{\frac{1}{3}}^2(\xi) \right\} \quad (1)$$

with

$$\gamma = \frac{W}{m_0 c^2}, \qquad \xi = \frac{2\pi}{3\gamma^3\lambda}[1+(\gamma\psi)^2]^{\frac{2}{3}}, \qquad \rho = \frac{W}{ecB}.$$

W, e, and m_0 are the energy, charge and rest mass of the electrons, I is the current of the electrons in the storage ring, B is the magnetic induction of the bending magnet at the tangent point of the electron beam to the observation point, and ψ is the opening angle between the orbital plane and the observation point. K_x is the modified Bessel function, order x of the the second kind, and c and ε_0 are fundamental constants. Thus, the spectral photon flux can be expressed in terms of eight measurable quantities:

$$\Phi_E = \Phi_E(E; W, B, I, \psi, \Sigma_y, d^{SR}, a, b) \quad (2)$$

where Σ_y characterizes the vertical size and divergence of the electron beam at the source point of the radiation, d^{SR} is the distance from the beam to the observation point, and a and b are the height and width of the limiting aperture. The other quantities are the same as above.

Horizontal variation of Φ_E is less than 10^{-3} over the width of the CCD.[9] Due to its dependence on the opening angle ψ, Φ_E varies strongly as the observation point moves out of the orbital plane of the electrons. Figure 3 shows how the synchrotron spectrum softens as the height above the orbital plane increases. The calculated Φ_E is for one electron in the storage ring with no chopper wheel. For typical integration times and ring currents, the detected flux above 4 keV was negligible.

A total of eleven devices were characterized during six separate 48 hour shifts. Typical measurements consisted of acquiring 2000 frames, with frame integration times in the range $0.83 - 1.53$ s , depending on which readout electronics were used. While storage ring currents varied from a minimum of 5 to a maximum of 50 electrons, the ring current was normally adjusted to either 10 or 20 electrons (again, dependent on the readout electronics) in order to ensure a flux of ~350 counts frame^{-1} quadrant^{-1} for a total of 3×10^6 counts in the $0.3 - 4.0$ keV band over the illuminated part of the CCD.

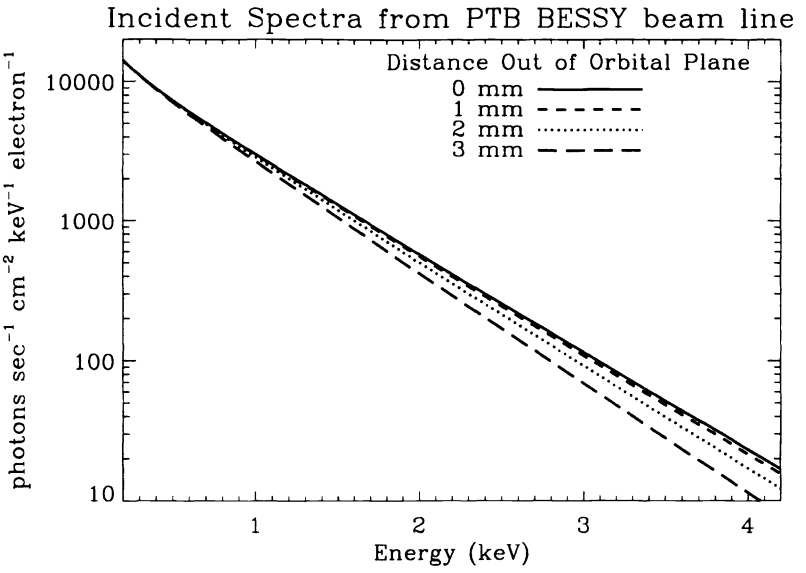

Figure 3. PTB White Light BESSY spectra as a function of height above the orbital plane.

3. ANALYSIS

Our approach to absolute CCD calibration follows that used, for example, by Scholze and Ulm[11] to calibrate a windowless Si(Li) detector. One assumes that the detector's spectral redistribution function is known, and that one knows the form of the detection efficiency as a function of energy. The parameters of the model detection efficiency are then determined from the data using a forward folding approach. That is, the known incident flux density is multiplied by a trial efficiency function and the result is convolved with the redistribution function and compared with the observed pulseheight distribution. Model parameters are adjusted until a satisfactory match between predicted and observed pulseheight distributions is obtained.

In this section we discuss our detector model and our data reduction pileup correction methods, and then present the best-fit detector model parameters.

3.1. Detector Model

We briefly review here the detector model we have used to analyze the synchrotron radiation data. The model contains a number of simplifying assumptions. The influence of these assumptions on the accuracy of our results is briefly discussed in §5.

It is convenient to describe the detector model in two parts. The detection efficiency model predicts the probability that an incident photon will interact in the device in such a way as to produce a valid, detectable event. The redistribution model predicts the pulse-height distribution of valid events obtained in response to a monochromatic incident beam. Here "valid" events are those which meet certain criteria designed to reduce detector background by discriminating between particle-induced and photon-induced events. For these measurements we use event selection criteria similar to those used in the ACIS flight instrument.

The detection efficiency model is the so-called "slab and stop model"[12] in which the complex CCD deadlayer structure[7] is greatly simplified. A sketch of one cross-section through the gate structure of these 3-phase CCDs is shown in Figure 4. Our model greatly simplifies this structure. In particular, the deadlayer over each pixel is assumed to consist of two regions: an electrode region and a channel-stop region. Within each region the deadlayer is taken to be a sandwich of layers, each homogeneous in planes parallel to the detector. Thus the electrode region of the deadlayer is modeled as a sandwich of Si, SiO_2, and Si_3N_4, while the channel stop region consists of deadlayers of Si and SiO_2. Two additional model parameters are the width of the pixel and the depletion depth.

Even in this simplified model, the parameters cannot be uniquely determined by the undispersed synchrotron radiation data alone. Instead, we rely on independently determined values from other experiments. In particular,

Prigozhin et al.[13] have measured the depletion depth at higher energies and we fix the depletion depth at the measured value in these fits. We note that the depletion depth is large enough that it does not strongly affect the response in the $0.3 - 4$ keV spectral band. The channel stop parameters have also been measured, using a mesh technique, as described by Pivovaroff et al.[14,15] Table 1 summarizes the model parameters.

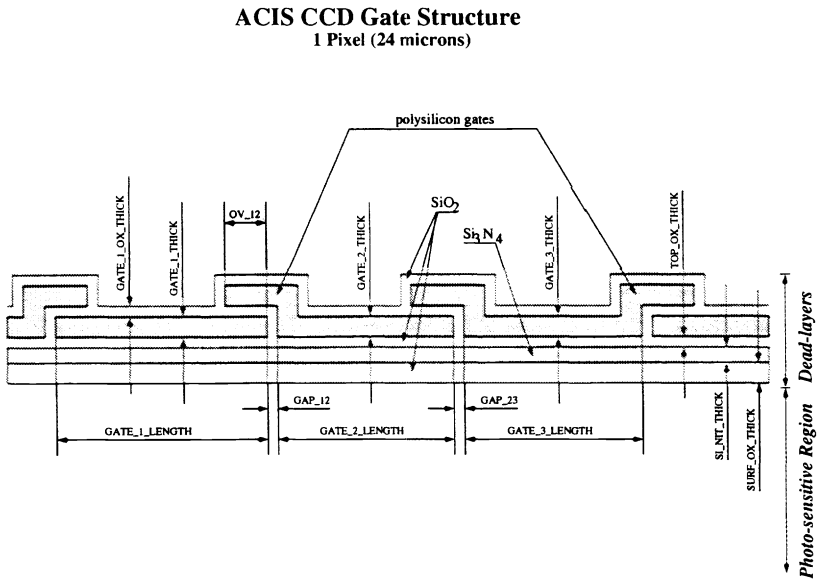

Figure 4. Cross section of the gate structure of the ACIS CCD along the transfer channel.

Table 1. CCD Detection Efficiency Model Parameters

Parameter Description	Status in Model Fits
Si gate thickness	varied
SiO_2 gate thickness	varied
Si_3N_4 gate thickness	varied
Depletion depth	fixed; determined by branching ratio method †
Channel stop width	fixed; determined by SEM measurements ‡
SiO_2 stop thickness	fixed; determined by SEM measurements ‡
Si p^+ thickness	fixed; determined by mesh experiments ‡
Pixel width	fixed at 24 μm design value

†: see references[13]
‡: see reference[14,15]

3.2. Data Reduction

We extract X-ray events from the raw data, saving the location, pulse-height value, and frame number of each event in an event list. The storage ring current log is consulted to identify periods between the (discontinuous) changes of the beam current, and the data are divided into sets of constant ring current. The pileup rate (discussed below) is quite sensitive to flux, and we analyze periods of different flux separately to permit the most accurate pileup correction. Finally, the event list is filtered by event shape ("grade") as it would be by the ACIS on-board processors. ASCA event grades 0,2,3,4 and 6 (essentially 1-, 2- and 3-pixel events) are accepted for this analysis. A pulse height spectrum of the filtered events is then generated.

In the analysis reported here, we integrate events within a 5 mm by 6 mm region of the detector. The predicted synchrotron flux is integrated over the corresponding angle. Thus, we integrate the spectrum within ± 2.5 mm of

the orbital plane of the storage ring. In our fits for detection efficiency model parameters we allow a single, energy-independent scale factor (or normalization) to modify the calculated incident flux density. This normalization parameter allows for events which penetrate the gate structure but are rejected as background events. The fraction of such events (which we may call the background branching ratio) is known to be 1% or lower in the zero-pileup limit, and essentially independent of energy in the $0.3 - 4$ keV band. Therefore the best fit value of the flux normalization is expected to greater than 0.99 but less than one.

3.3. Pileup Correction

If the storage ring current is sufficiently high, pileup may affect both the shape and normalization of the pulse-height spectrum. We have used a model that relies on extensive laboratory data and first principles to correct the effects of pile-up. The details of this method are explained in detail elsewhere.[16] Here we summarize this technique and its application to the analysis of our absolute calibration.

Pile-up modifies the apparent energy and shape (or "grade") of detected X-ray events. The mechanism modifying the apparent energy is the obvious one: if two photons interact within the same pixel during a single exposure, the resulting charge cloud may be ascribed erroneously to a single event of incorrect energy. The event shape modification can occur if two photons land in adjacent pixels, and in this case the incident photons might not be detected at all. This can happen if such piled-up events are mistaken for particle background events and are thus rejected by the event selection algorithm.

The probability of such redistributions was determined as a function of energy[16] from pseudo-monochromatic measurements at twelve energies spanning $1.4 - 10$ keV, each containing a series of measurements over a wide range of incident fluxes, from a low flux limit with no pileup to a high flux limit with significant pileup. This information was then interpolated and folded into a model that allows the correction of polychromatic or continuous spectra.

Figure 5 shows a pulse-height spectrum with a beam current of 19 electrons. The spectrally integrated flux (from $0.3 - 4$ keV) for a typical exposure was approximately 60 events s^{-1} cm^{-2} per electron of beam current. At a typical fluence (for 19 electron beam current and a 1.526 s exposure time) of 5×10^{-3} events $pixel^{-1}$ $frametime^{-1}$, approximately 3% of all events were lost to pileup.

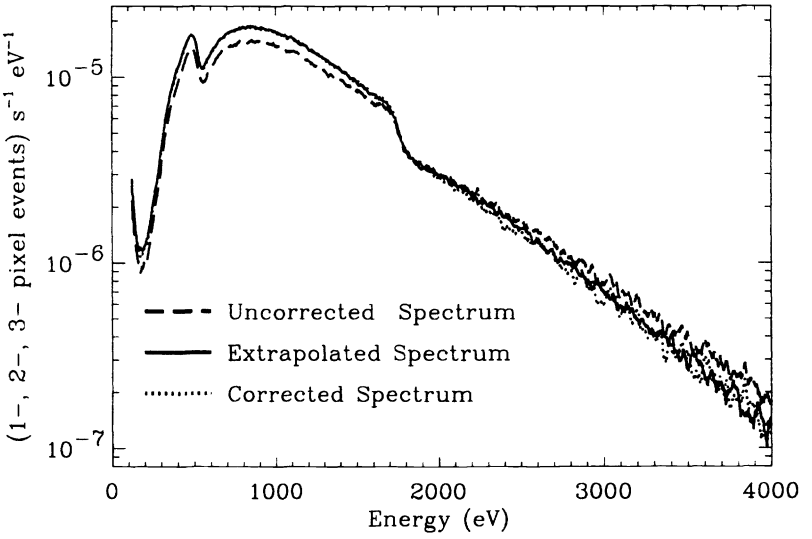

Figure 5. PTB white light BESSY spectra. The graph compares the raw, "uncorrected" piled-up spectrum, to two methods of pileup correction: "corrected", using a first principles approach with laboratory data, and "extrapolated", using a channel-by-channel interpolation to the zero storage ring current limit, and hence no pileup limit. The agreement between the two correction methods is very good.

Spectrally, the effects of pile-up appear as a deficiency of low-energy events and an excess high-energy flux. As a check on the pileup model, we have compared the pileup-corrected spectrum with a channel-by-channel linear

extrapolation of the observed pulseheight spectrum to zero storage ring current; as is shown in Figure 5, the agreement is excellent.

3.4. Fitting Results

The predicted synchrotron spectrum (with free normalization) and the CCD efficiency model are fit to the pileup-corrected pulseheight spectrum using the **XSPEC**[17] spectral fitting package. The CCD model parameters are varied to minimize the chi-squared associated with the fit. Parameters are allowed to vary or are fixed in the fits according to Table 1. Only data in the spectral range $0.3 - 4$ keV are considered in these fits.

Figure 7, Figure 8, and Figure 6 show the best fit models with the data for individual quadrants of detectors w190c3, w190c1, and w103c4. Table 2 shows the best-fit parameters, the RMS error, and the normalization accuracy for each reference detector as well as listing the values of parameters held constant in the fitting process.

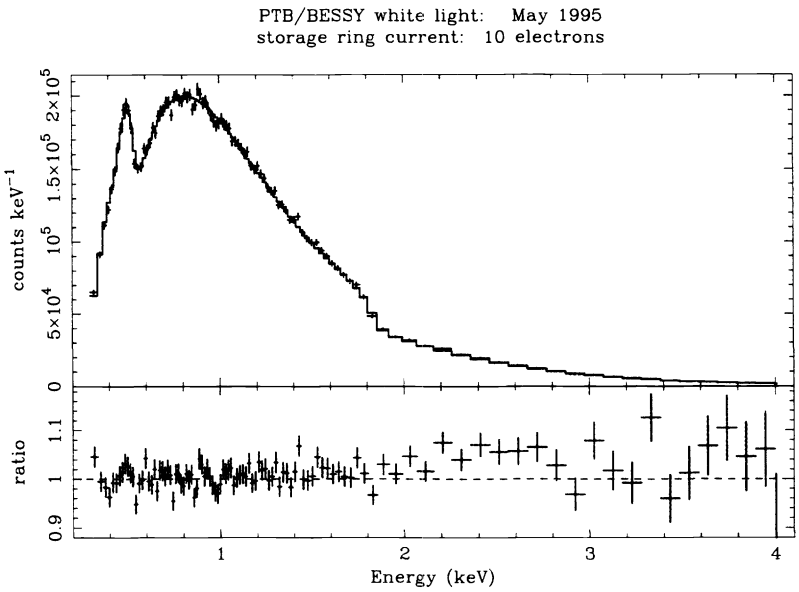

Figure 6. Observed pulse-height distribution and best-fit model from undispersed synchrotron radiation measurements for device w103c4, quadrant B. The data are an accumulation of 975 exposures, each with integration time 1.526 s, taken with a storage ring current of 10 electrons.

	Free				Fixed				RMS Fit	
Chip	Si†	SiO_2‡	Si_3N_4	Normalization	CS Si	CS SiO_2	CS Width	Depl. Depth	Residual	χ^2_ν/dof
w190c3	0.259	0.354	0.031	$0.999 \pm .005$	0.35	0.45	4.1	71.3	2.54%	1.227/875
w190c1	0.261	0.358	0.029	$0.993 \pm .005$	0.35	0.45	4.1	70.6	2.26%	1.094/916
w103c4	0.291	0.202	0.030	$0.947 \pm .005$	0.35	0.45	4.1	57.9	3.74%	1.380/1807

Note: All thicknesses are in μm. χ^2_ν is the reduced χ^2 value, where ν is the degrees of freedom. Normalization uncertainties reported are the 90% confidence limits from fitting. Uncertainty in the expected normalization value is 0.001.

† typical 90% confidence limit is ± 0.008 μm

‡ typical 90% confidence limit is ± 0.011 μm

Table 2. CCD model parameter fit results from synchrotron radiation measurements

The model fits for all three CCDs are reasonably good, although devices w190c1 and w190c3 have lower RMS values than w103c4. The most prominent systematic trend in the residuals (the ratio of data to model) is a feature around 1.8 keV. An underestimation of the Si Kα fluorescence could help contribute to the narrow feature. Analysis of

the response function model suggests that it underestimates the fluorescence line strength. Another potential source of error is the use of the Henke[21] optical constants in the current detector model. Our EXAFS measurements[18] show large deviations from the tabulated Henke values around both the O Kα and S Kα absorption edges.

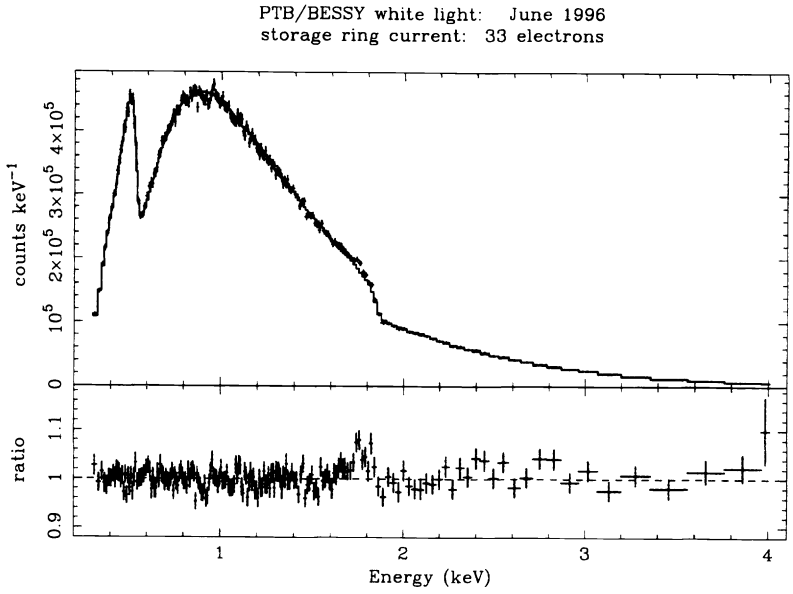

Figure 7. Observed pulse-height distribution and best-fit model from undispersed synchrotron radiation measurements for device w190c1, quadrant A. The data are an accumulation of 1483 exposures, each with integration time 0.848 s, taken with a storage ring current of 33 electrons.

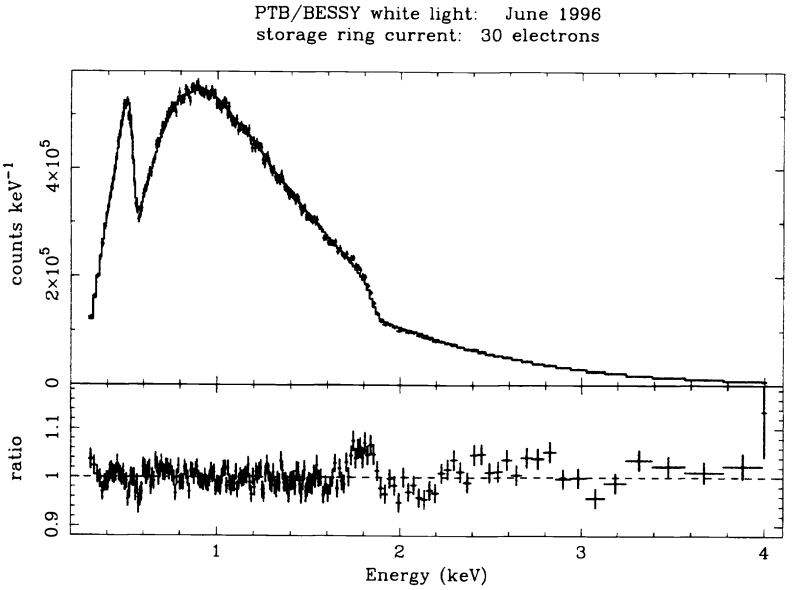

Figure 8. Observed pulse-height distribution and best-fit model from undispersed synchrotron radiation measurements for device w190c3, quadrant B. The data are an accumulation of 2000 exposures, each with integration time 0.813 s, taken with a storage ring current of 30 electrons.

For devices w190c1 and w190c3, the best-fit normalizations are within 1% of unity, while for w103c4 the normalization is 0.95. The reason for this discrepancy is not understood. The w103c4 data were obtained with an early generation of detector electronics which provided slower readout, lower gate bias (and hence, lower depletion depth) and slightly higher noise than the flight-like electronics used with the other two detectors. The pileup corrections for the two data sets are comparable, since the storage ring current was adjusted to compensate for the difference in frame exposure times. However, the effective exposure time determination (see §2) is less certain for the shorter exposure time. In principle, the normalization differences could be variations in the valid-event branching ratios of the two devices, although the relative quantum efficiency measurements discussed below are not consistent with this hypothesis. It should be noted that the w103c4 data were obtained a year earlier than the the w190c3 and w190c1 data.

It is interesting to compare the best-fit parameters for chips w190c1 and w190c3. These two CCDs were produced on the same silicon wafer, so they should have similar gate thicknesses. The differences between the derived thickness for the Si, SiO_2, and Si_3N_4 layers are well within the statistical errors.

3.5. Spatial Uniformity

Extensive measurements at MIT CSR[4] have shown that the spatial variation of quantum efficiency, for front-illuminated devices, is quite small (< 2%, RMS) on scales as small as 0.77 mm^2. Because the intensity and shape of the synchrotron spectrum changes over the illuminated detector area, we have not attempted to constrain the small-scale uniformity of the reference detectors directly from the synchrotron measurements. On larger scales, however, we confirm that the detector response is extremely uniform.

Figure 9 (*left*) shows the cumulative intensity map obtained for w190c1 during the June 1996 user session. The storage ring current was constant at 15 electrons as each of five subsections of the detector was illuminated during this experiment. The variation in the vertical direction is real reflects the variation in the synchrotron radiation as a function of the opening angle ψ (see Equations 1 & 2 and Figure 5). The dark vertical gaps are either quadrant boundaries or defective columns. The mean counting rate is ~12 events $pixel^{-1}$. Figure 9 (*right*) plots the same data, but summed in the direction parallel to the quadrant boundaries. The uniformity of the detector is evident, with the only deviations from linearity being due to boundaries or bad columns. We note that ACIS flight detectors generally have much higher cosmetic quality than this reference detector.

Table 3 shows the average current-normalized counting rate (cts sec^{-1} $electron^{-1}$ ring current), for each quadrant of w190c1 at four different CCD positions. Each position is labeled by the location of the first row exposed in the measurement (e.g., the y209 data illuminated rows 209−417); the data are normalized by the value measured at y001. The defective columns have been removed for this analysis. Excepting the y768/quad D value (a suspect data point given the numerous defective columns there), the mean of the values in the table is 1.000 and the sample deviation is 0.003. The expected photon counting errors are of order 0.001 in relative efficiency. These results demonstrate that the broad-band responsivity of the CCDs in the 0.3 − 4 keV spectral band varies by less than 1% on spatial scales of 5 mm.

CCD Position	Quad A	Quad B	Quad C	Quad D
y209	0.999	0.997	0.998	1.003
y417	1.003	1.002	1.004	1.008
y625	1.000	1.001	1.002	1.000
y768	0.998	0.996	1.002	0.978

Table 3. Average counting rate per quadrant per exposure time (for ASCA grades 02346) at four positions on device w190c1, relative to that at CCD position y001. As the storage ring current was 15 electrons for each measurement, no pile-up correction was required for this uniformity measurement. Defective columns (see Figure 9) have been accounted for. Statistical errors for all measurements are 0.001. This data was acquired with the first-generation (non-flight) electronics in June, 1996.

4. QUANTUM EFFICIENCY OF FLIGHT DETECTORS RELATIVE TO REFERENCE DETECTORS

We measured the detection efficiency of the ACIS flight CCDs, relative to the absolutely calibrated standard detectors, using apparatus and methods described elsewhere.[3,19] Briefly, in these measurements both flight and reference detectors are illuminated by a quasi-monochromatic, temporally stable, diffuse X-ray beam of selectable energy. Measurement energies range from 0.277 keV to 8.9 keV. Since different physical processes are used to produce the X-rays at different energies, the spectral purity and spatial uniformity of the beam vary from energy to energy. Our use of CCD reference detectors, which have spectral and spatial resolution nearly identical to that of the flight devices being calibrated, allows us to measure and monitor the beam pattern and spectral content. This capability minimizes systematic errors associated with spectral and spatial complexities of the sources.

The relative quantum efficiency measurements are used, together with the best-fit response model of the standard detectors, to fit models of the flight detector quantum efficiency. The same detector model is used to describe the flight detector response as was used for the reference detectors.

While the primary motivation for measuring the quantum efficiency of the flight detectors relative to the reference standards was of course to characterize the flight detectors, we can also use these measurements as a consistency check on the calibration of the reference detectors. We can do this because the detection efficiency of the flight detectors, relative to one another, has been extensively characterized during instrument level testing at the X-ray Calibration Facility (XRCF) at Marshall Space Flight Center.[20] The repeatability of our relative quantum efficiency measurements (at both MIT CSR and XRCF) suggests that the (spatially averaged) relative efficiency of two detectors can be determined with an RMS error of 0.6% at energies less than 6 keV.

5. QUANTUM EFFICIENCY ACCURACY

In this section we discuss the accuracy of our absolute detection efficiency measurements. Our principal quantitative check on the these measurements is to place to calibrated devices in the same beam and compare their observed responses with the predictions of the absolute response model for each. We do this at two levels: first, by directly

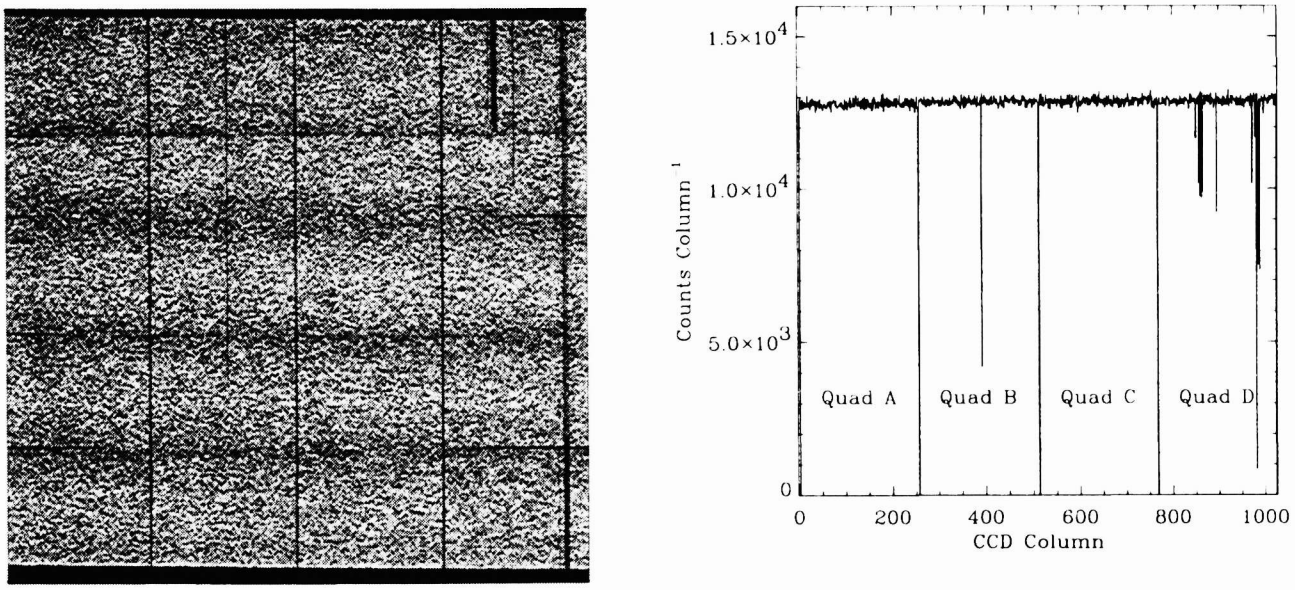

Figure 9. PTB/BESSY data for w190c1 (June, 1996). **LEFT:** Intensity map of total counts from a series of five observations illuminating different portions of the detector. The pattern in the vertical direction reflects the variation in synchrotron radiation intensity as a function of distance out of the orbital plane. Dark vertical features are either quadrant boundaries or defective columns. **RIGHT:** A plot showing the same data to the left summed in the direction parallel to the quadrant boundaries. The only significant deviations from uniformity are due to the quadrant boundaries or defective columns.

comparing the responses of two transfer-standard detectors that have been calibrated at PTB and second, by comparing the responses of flight model detectors which have been calibrated with respect to the transfer standard detectors.

5.1. Relative Efficiencies of Transfer Standard Detectors

Reference standard detectors w190c3 and w103c4 were calibrated with respect to one another at MIT CSR using the procedures described above for calibration of the flight detectors relative to the reference standards. The relative efficiencies so obtained were compared to the predictions of models derived from the (separate) synchrotron measurements of these two devices. Results are shown in Figure 10. The upper panel of this figure shows the absolute quantum efficiencies determined from the synchrotron data. The higher efficiency of w103c4 is attributable to its relatively thin gate oxide layer. The model quantum efficiencies plotted here include no correction for the normalization differences listed in Table 2. The bottom panel of Figure 10 shows the discrete relative measurements made at MIT CSR *vs.* the expectations from the synchrotron calibration.

The ratio of the two models agrees quite well with the relative quantum efficiency data: for the five energies measured at MIT within the BESSY passband (0.525 to 4.5 keV), the residuals (measured ratio minus modeled ratio) have a mean of -0.008 and a standard deviation of 0.01. Thus the mean is consistent with 0 at the 2-sigma level, provided the standard deviation is taken to be measure of the random errors in the residuals. The latter assumption is a good one, given that the errors in the relative quantum efficiency measurements are thought to have a standard deviation of 0.6%. This result suggests that the normalization differences required by the best fits to the synchrotron data do not result from differences in the reponses of the detectors. Instead, they suggest the presence of some as-yet unmodelled effect in the synchrotron measurements.

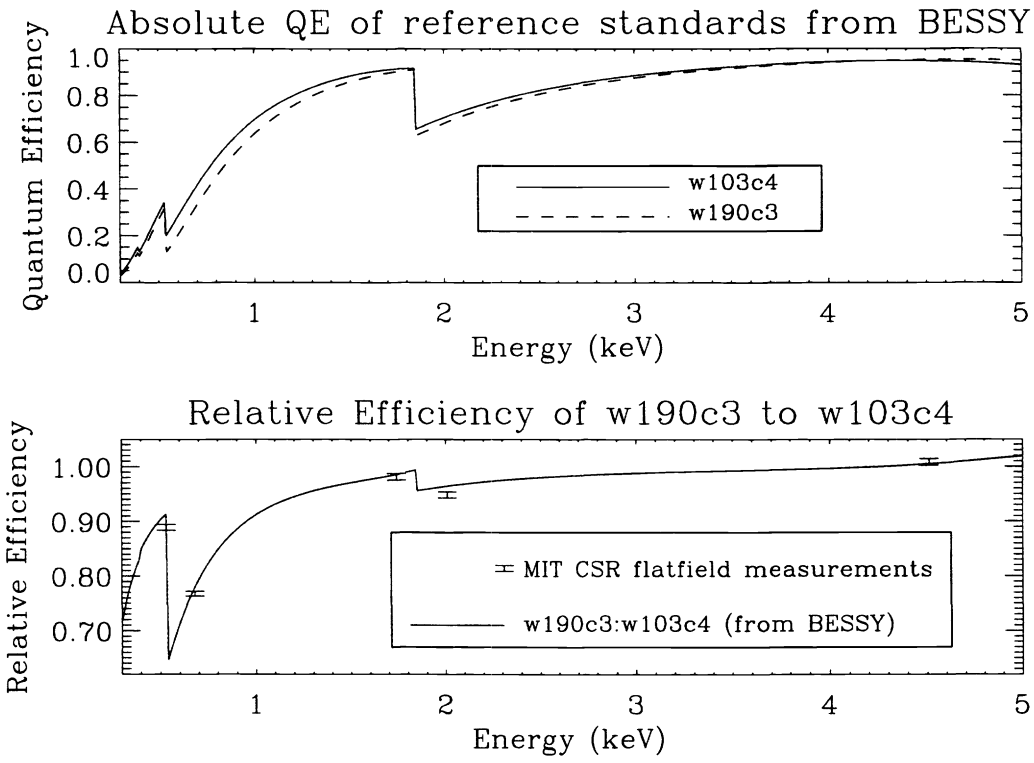

Figure 10. PTB/BESSY absolute efficiencies vs. MIT CSR relative efficiencies for reference detectors w190c3 and w103c4.

5.2. Relative Efficiencies of Flight Detectors

As a check on the accuracy of the quantum efficiency models derived for each of the flight detectors, and indirectly on the accuracy of the reference detector calibration, we used an independent set of relative efficiency data obtained during integrated instrument testing at Marshall Space Flight Center's X-ray Calibration Facility (XRCF). In these tests the entire focal plane was illuminated by various electron impact sources. The source-to-detector distance (over 500 m) ensured an extremely uniform beam at the ACIS focal plane. *Chandra's* High-Resolution Mirror Assembly was not in the beam during these "flat-field" measurements.

We arbitrarily selected one of the ACIS front-illuminated detectors (the S2 detector) to use as a beam normalization detector, and then computed the efficiency of each of the other seven front-illuminated detectors relative to S2. These relative efficiency ratios were compared to the predictions of the respective detector response models derived from calibration of the flight detectors relative to the transfer standards. Specifically, we define, for each detector i, the best-fit model quantum efficiency to be $q_i(E)$, and the XRCF-measured counting rate to be $c_i(E)$, both at energy E. We then compute the ratio differences

$$\delta_i(E) \equiv \frac{c_i(E)}{c_{S2}(E)} - \frac{q_i(E)}{q_{S2}(E)}$$

We plot the ratio differences $\delta_i(E)$ as a function of energy in Figure 11 for each of seven detectors. The error bars on these points represent the statistical errors associated with each measurement. The RMS value of the points at energies greater than or equal to 525 eV is 1.3%.

The solid lines in Figure 11 provide an estimate the 90% confidence intervals for the model predictions. These limits are derived from the (correlated) errors in the efficiency model parameters determined from fits to the data relative quantum efficiency data. We have neglected uncertainties in the fixed parameters (e.g., the channel stop parameters) in formulating these confidence limits. The confidence limits become quite large below 525 eV because the flight detectors were not calibrated relative to the transfer standards at lower energies. The CCD detection efficiency is falling quite rapidly as the photon energy decreases below 400 eV, and is much less than 1% at 277 eV. The estimated model confidence intervals bound the observations well.

5.3. Discussion

We have identified quantitative bounds on systematic measurement errors and on some kinds of modeling errors. Taken together, these checks furnish confidence that, for front-illuminated devices, the absolute quantum efficiency errors are smaller than 5% in the $0.3 - 4$ keV band. Narrow band efficiency measurements are probably accurate to better than 1.5%, except at energies in the immediate vicinity of the characteristic silicon absorption edges. We summarize the evidence for these assertions as follows:

1. *Plausibility of best-fit model parameters.* The best-fit values for synchrotron radiation flux normalizations, relative to the expected value, for three reference detectors discussed earlier in §3.4 are 0.999,0.994, and 0.947, respectively; these numbers each formal have 90% confidence intervals of approximately ±0.005. The largest known systematic uncertainty is the background grade branching ratio, which may contribute an uncertainty of 1% in the normalization. The simplest interpretation of these results is that any residual systematic errors in the broad-band quantum efficiency amount to less than 5%. Moreover, the inferred mean gate structure parameters are in the range (within ±50%) expected given the device fabrication process, suggesting that the slab and stop model is providing a reliable representation of the gate structure.

   It must be recognized, however, that the dispersion in the values of flux normalization required to fit the storage ring data is larger than can be explained on the basis of known measurement errors. As is discussed above in § 5.1, the relative quantum efficiencies of the detectors are consistent with models derived from the storage ring data to much better than 5% tolerance. Under these circumstances, we regard as conservative our estimate that the absolute flux calibration of ACIS is uncertain at the 5% level.

2. *Internal consistency of measured and modeled relative detector quantum efficiencies.* The quantum efficiency models derived for the reference detectors from synchrotron radiation measurements predict the relative efficiency measurements made at MIT CSR with an accuracy of better than 2%. Moreover, the relative efficiency of the various flight detectors is also consistent, with better than 1.5% RMS error, with efficiency models derived from the synchrotron radiation measurements. These results are consistent with the spectral distribution of the residuals observed in fits to undispersed synchrotron data for the reference detectors.

5.4. Model Limitations

The absolute detection efficiency errors reported here, while quite small by the standards of X-ray astronomy, are much larger than one would expect on the basis of photon-counting errors alone. In this section, we briefly enumerate factors which may limit the accuracy of the detector models derived from these measurements.

1. *The gate structure model is oversimplified.* The slab and stop model ignores gate overlaps and phase-to-phase variations in gate thickness. The resulting error varies in lowest order as the square of the optical depth of the gate structure, so in the limit that the gates are optically thin, the error vanishes. Conversely, the magnitude of this error is largest just above the absorption edges of oxygen and silicon, and at very low energies. It is interesting to note in this connection that the systematic deviations near the absorption edges in Figures 7 through 6 are smallest for w103c4, the device with the smallest gate opacity.

2. *Absorption fine-structure was ignored in determining model parameters.* The undispersed synchrotron radiation data were analyzed using standard Henke[21] absorption coefficients; these omit edge structure which we have since measured.[18] While the spectral resolution of the detector tends to smooth the fine structure, we have not yet established the magnitude of error introduced by neglect of fine structure. The relatively large residuals from the best-fit model near the absorption edges probably reflect this error.

3. *The redistribution function is oversimplified.* A phenomenological representation of the spectral redistribution function has been used in analysis of synchrotron radiation data. The response to a monochromatic input

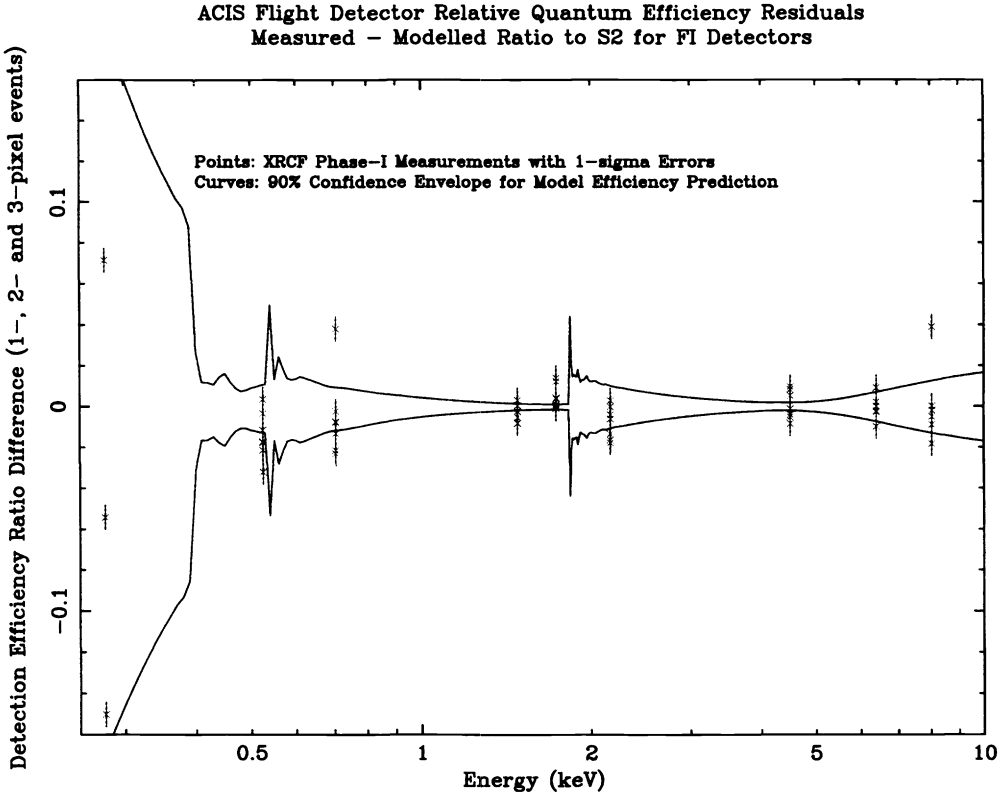

Figure 11. Comparison of XRCF relative quantum efficiency measurements to Model Predictions for front-illuminated detectors from "flatfield" measurements. Points are deviations between XRCF quantum efficiency measurements, relative to S2, and the corresponding efficiency ratio predicted from the absolute efficiency calibration. Solid lines are estimated 90% confidence intervals for model predictions. Note that the models are based entirely on relative QE measurements made at MIT; the points shown were NOT used to constrain the models. The RMS of the residuals for energies $\geq$ 525 eV is 1.3%.

is modeled as the sum of several Gaussians plus a phenomenological low-energy tail. A better, physically-grounded model of the redistribution function is now available,[22] but has not yet been used to analyze the synchrotron data.

4. *Channel stop parameter values have not been measured directly for the reference detectors.* The most reliable measurements of channel stop dimensions are obtained using the mesh techniques[14,15] and from (destructive) scanning electron micrographs. Neither of these techniques has been applied to determine the channel stop parameters of the reference detectors themselves. It is hoped that mesh measurements can be made on at least one of the reference detectors.

6. SUMMARY

We have used undispersed synchrotron radiation from the PTB beamline at the BESSY I electron storage ring to measure the absolute X-ray detection efficiency of CCDs employed in *Chandra's* ACIS instrument. We believe broad-band ($0.3-4$ keV) efficiency errors are less than 5%. Narrowband flux measurements appear to be accurate to better than 2%. Accuracy is expected to be poorest near the absorption edges of oxygen and silicon. The accuracy is probably limited by simplifications in the gate structure model and in the variation of absorption coefficients with energy. Re-analysis of these data with more complex detector models would probably improve ACIS calibration accuracy. We observe that, given the extremely good spatial uniformity of the ACIS detectors, future high-accuracy CCD calibration programs might benefit from synchrotron radiation measurements with mesh masks. The resulting subpixel resolution would probably reduce the largest systematic errors remaining in the analysis presented here.

ACKNOWLEDGMENTS

ACIS Instrument calibration was the work of many people. We acknowledge especially Beverly Fergason LaMarr, Herb Manning and Paul Plucinsky for intense work at MIT CSR on the relative efficiency calibration, and Martin Weisskopf and the *Chandra* Project Science team for creating and operating the NASA MSFC X-ray Calibration Facility. The ACIS Principal Investigator is Dr. Gordon P. Garmire of the Pennsylvania State University, without whom ACIS calibration would not have been possible. The entire ACIS team at Penn State and MIT contributed to the calibration of ACIS at the XRCF. This work was funded by NASA through contract NAS8-37716.

REFERENCES

1. M. Weisskopf, H. D. Tananbaum, L. P. Van Speybroeck, and S. L. O'Dell, These proceedings
2. F. A. Jansen, These proceedings
3. M. W. Bautz, S. E. Kissel, G. Y. Prigozhin, S. E. Jones, T. Isobe, H. L. Manning, M. Pivavaroff, G. R. Ricker, and J. Woo, "X-ray CCD calibration for the AXAF CCD Imaging Spectrometer," in *Proc. SPIE*, vol. 2808, pp. 170–181, Oct. 1996.
4. M. W. Bautz, M. Pivovaroff, F. Baganoff, T. Isobe, S. E. Jones, S. E. Kissel, B. Lamarr, H. L. Manning, G. Y. Prigozhin, G. R. Ricker, J. A. Nousek, C. E. Grant, K. Nishikida, F. Scholze, R. Thornagel, and G. Ulm, "X-ray CCD calibration for the AXAF CCD Imaging Spectrometer," in *Proc. SPIE*, vol. 3444, pp. 210–224, Nov. 1998.
5. M. W. Bautz, G. Y. Prigozhin, M. J. Pivovaroff, S. E. Jones, S. E. Kissel, and G. Ricker, "X-ray CCD response functions, front to back," *Nucl. Inst. Meth. A* **436**, pp. 40–52, Oct. 1999.
6. G. Garmire. In preparation, 2000.
7. B. E. Burke, J. Gregory, M. W. Bautz, G. Y. Prigozhin, S. E. Kissel, B. B. Kosicki, A. H. Loomis, and D. J. Young, "Soft X-Ray CCD Imagers for AXAF," *I. E. E. E. Trans. Elec. Devices* **44**, pp. 1633–1642, Oct. 1997.
8. G. Arnold, D. & Ulm, "Electron storage ring BESSY as a source of calculable spectral photon flux in the x-ray region," *Rev. Sci. Instrum.* **63**, p. 1, Jan. 1992.
9. F. Riehle and B. Wende, "Establishment of a spectral irradiance scale in the visible and near infrared using the electron storage ring BESSY," *Metrologia* **22**, pp. 75–85, 1986.
10. J. Schwinger, "On the classical radiation of accelerated electrons," *Phys. Rev.* **75**, pp. 1912–1925, 1949.
11. F. Scholze and G. Ulm, "Characterization of a windowless Si(Li) detector in the photon energy range 0.1 - 5 keV," *Nucl. Inst. Meth. A* **339**, pp. 49–54, June 1994.
12. K. C. Gendreau, *X-ray CCDs for Space Applicatinos: Calibration, Radiation Harness, and Use for Measuring the Spectrum of the Cosmic X-ray Background.* PhD thesis, Massachusetts Institute of Technology, 1995.

13. G. Y. Prigozhin, K. Gendreau, M. Bautz, B. Burke, and G. Ricker, "The Depletion Depth of High Resitivity X-ray CCDs," *I. E. E. E. Trans. Nuc. Sci.* **45**, pp. 903–90, June 1998.
14. M. Pivovaroff, S. Jones, M. Bautz, S. Kissel, G. Prigozhin, G. Ricker, H. Tsunemi, and E. Miyata, "Measurement of the Subpixel Structure of AXAF CCD's," *I. E. E. E. Trans. Nuc. Sci.* **45**, pp. 164–175, Apr. 1998.
15. M. Pivovaroff, S. Kissel, G. Prigozhin, M. Bautz, and G. Ricker, "In situ measurement of the channel stop structure in AXAF CCDs," in *Proc. SPIE*, vol. 3765, pp. 278–284, Nov. 1999.
16. S. Jones. In preparation, 2000.
17. K. Arnaud, "The XSPEC Spectral Fitting Program," in *Astronomical Data Analysis Software and Systems, V; ASP Conference Series*, G. Jacoby and J. Barnes, eds., vol. 101, p. 17, 1996.
18. G. Prigozhin, J. Woo, J. Gregory, A. Loomis, M. Bautz, G. Ricker, and S. Kraft, "X-ray absorption near edge structure in quantum efficiency of X-ray CCDs," *Optical Engineering* **37**, pp. 2848–2854, Oct. 1998.
19. S. E. Jones, M. W. Bautz, S. E. Kissel, and M. Pivovaroff, "Using tritium and X-ray tubes as X-ray calibration sources for the AXAF CCD Imaging Spectrometer," in *Proc. SPIE*, vol. 2808, pp. 158–169, Oct. 1996.
20. M. C. Weisskopf and S. L. O'Dell, "Advanced X-ray Astrophysics Facility (AXAF): Calibration overview," in *Proc. SPIE*, R. B. Hoover and A. B. Walker, eds., vol. 3113, pp. 2–18, July 1998.
21. B. L. Henke, E. M. Gullikson, and J. C. Davis, "X-ray interactions: photoabsorption, scattering, transmission, and reflection at E=50-30000 eV, Z=1-92," *Atom. Data Nucl. Data Tables* **5**, pp. 181–342, July 1993.
22. G. Prigozhin, S. Jones, M. Bautz, G. Ricker, and S. Kraft, "Physics of the Low Energy Tail in the ACIS CCD. The Spectral Redistribution Funciton," *Nucl. Inst. Meth. A* **439**, pp. 582–591, Apr. 2000.